# The Molecular Structure of the Liquid Ordered Phase of Lipid Bilayers

**Alexander J. Sodt**[1], **Michael Logan Sandar**[2], **Klaus Gawrisch**[3], **Richard W. Pastor**[1], and **Edward Lyman**[2,4,*]

[1]National Heart, Lung, and Blood Institute, National Institutes of Health, Bethesda, MD

[2]Department of Physics and Astrophysics, University of Delaware, Newark, DE

[3]National Institute on Alcohol Abuse and Alcoholism, National Institutes of Health, Bethesda, MD

[4]Department of Chemistry and Biochemistry, University of Delaware, Newark, DE

## Abstract

Molecular dynamics simulations reveal substructures within the liquid-ordered phase of lipid bilayers. These substructures, identified in a 10 μsec all-atom trajectory of liquid-ordered/liquid-disordered coexistence ($L_o/L_d$), are composed of saturated hydrocarbon chains packed with local hexagonal order, and separated by interstitial regions enriched in cholesterol and unsaturated chains. Lipid hydrocarbon chain order parameters calculated from the $L_o$ phase are in excellent agreement with $^2$H NMR measurements; the local hexagonal packing is also consistent with $^1$H-MAS NMR spectra of the $L_o$ phase, NMR diffusion experiments, and small angle X-ray- and neutron scattering. The balance of cholesterol-rich to local hexagonal order is proposed to control the partitioning of membrane components into the $L_o$ regions. The latter have been frequently associated with formation of so-called rafts, platforms in the plasma membranes of cells that facilitate interaction between components of signaling pathways.

### Keywords

lipid rafts; cholesterol; molecular dynamics; Hidden Markov Model

## INTRODUCTION

Two phase coexistence in binary mixtures of a lipid with cholesterol was first observed in the early 1970s.[1] More recently, coexisting *liquid phases*, known as "liquid ordered" ($L_o$) and "liquid disordered" (here called $L_d$, sometimes called $L_\alpha$) in cholesterol containing mixtures of three components have been studied extensively.[2–4] The $L_o$ phase[5] shares features with raft domains in cell membranes[6–8] — it is enriched in saturated lipids and is cholesterol dependent. Experimental evidence for rafts in resting cell membranes is consistent with sizes less than 30 nm.[9,10] Nanometer scale $L_o$ domains are found near a

miscibility critical point;[11–13] nanoscale domains are also observed in lipid mixtures containing lipids with a single unsaturated chain.[14–17] However, it is almost universally reported that membrane components which partition into the raft phase in the cell membrane partition out of the $L_o$ phase in ternary mixtures.[6]

Despite a wealth of experimental data, the detailed molecular structure of nanoscale domains in the $L_o/L_d$ two-phase region remains unknown. Ultimately, molecular scale structure and interactions drive partitioning of membrane components, and knowledge of them will help establish connections between the $L_o$ phase in model membranes and rafts in live cells. The goal of this work is therefore to elucidate the molecular structure of the $L_o$ phase.

An extensive body of molecular dynamics (MD) simulation literature has considered the effect of cholesterol on bilayers (see review by Róg, et al.[18]), including recent simulations of binary[19–22] and ternary mixtures.[23–25] While an important first step, these results cannot provide strong evidence for liquid-liquid phase separation, since conventional "all-atom" MD timescales have so far been insufficient to sample lipid mixing degrees of freedom. This is clear, based on the diffusion of individual lipids — on the timescale of 100 nsec, a lipid with a diffusion coefficient of $10^{-7}$ $cm^2$/sec covers an area of 12 $nm^2$ which is significantly smaller than the size of a typical membrane patch in simulations. Furthermore, lateral heterogeneity of lipid distribution may slow mixing relative to this naive estimate.[26] However, on the timescale of 10 μsec, as used in this study, an area of 1.2 $μm^2$ is covered which is much larger and potentially sufficient to achieve an equilibrium lateral distribution of lipids. (Limited mixing of lipid components, may be effected by advanced techniques,[27] at the expense of realistic dynamics.)

Ten μsec all atom simulations of a ternary mixture of dioleyoylphosphatidylcholine (DOPC), dipalmitoylphosphatidylcholine, (DPPC), and cholesterol obtained on the An-ton special purpose computer[28] are presented. At a temperature just below the miscibility transition (denoted by $T_m$), robust $L_o/L_d$ coexistence is observed despite extensive lipid mixing, and is confirmed by comparison of lipid chain order parameters from the simulation to measured $^2H$ NMR quadrupolar splittings and by control simulations of the homogeneous phases. The simulations reveal previously unobserved substructure within the $L_o$ phase comprised of saturated chains packed in transient regions of local hexagonal order. The substructure within the $L_o$ phase suggests an alternate view on the molecular mechanisms that drive liquid-liquid phase separation, and provides insight into partitioning of membrane components into the $L_o$ phase.

## METHODS AND MODELS

### Building the initial configuration

Two separate bilayer systems were built with the CHARMM-GUI, one with an $L_o$ composition and one with an $L_d$ composition.[29] The compositions were taken from published experimental results for a 1:1 ratio of DOPC:DPPC + 20 mol % chol at 298 K.[13] The $L_o$ system comprised 76 DOPC, 280 DPPC, and 156 CHOL, and the $L_d$ system 240 DOPC, 116 DPPC, and 44 CHOL. Each bilayer was simulated in the constant particle number, pressure, and temperature ensemble (NPT) until the membrane area equilibrated.

The initial configuration for the $L_o/L_d$ system was then created by embedding a 5 nm diameter, roughly circular patch of the equilibrated $L_o$ bilayer into the equilibrated $L_d$ bilayer, and eliminating any overlapping lipids from the $L_d$ bilayer (Figure S1). Care was taken both to maintain the correct composition of each region and to obtain a symmetric bilayer during this process. After embedding the $L_o$ domain and symmetrizing the bilayer, the final number of lipids of each type was 174 DOPC, 114 DPPC, and 60 CHOL. This gives a bulk composition that is closer to 1:1.5 +20% DOPC:DPPC + CHOL, but since the miscibility transition temperature and compositions of each phase are only weakly dependent on the DOPC fraction,[13] we expect this deviation to have a minor effect. A water box containing 16,261 waters and 0.150 M NaCl was added. The resulting system was allowed to relax under NPT conditions again, while weakly restraining the lipid headgroups to maintain the monolayers and also prevent water from entering the gap between the $L_o$ and $L_d$ regions. After the system area had relaxed, the restraints were removed, and system was relaxed for just over 25 nanoseconds of unrestrained NPT simulation. The end result of this procedure is shown in Figure S1, panel C. An initial configuration for a control simulation for the high temperature, mixed phase was built with the CHARMM-GUI, this time simply choosing the positions of all three components randomly.

## Production simulation on Anton

Anton is a special purpose machine designed for high performance molecular dynamics calculations. Details on the Anton machine can be found elsewhere [30]. The equations of motion were integrated with the Verlet algorithm with a timestep of 2.0 fsec. A constant temperature and a pressure of 1 atm were maintained by the Martyna-Tobias-Klein method,[31] with the pressure coupling effected every 240 fsec and the temperature coupling every 24 fsec. The temperature of the system initiated from a phase separated state was maintained at 298 K, the temperature of the homogeneous system was maintained at 328 K. Lennard-Jones interactions were truncated at 10.14 Å by a hard cutoff with no shift. Long range electrostatics were computed by the k-space Gaussian split Ewald method[32] on a 64×64×64 point grid, with the parameters of the Gaussian chosen to yield a root mean squared error in the electrostatic force calculation of 0.18%. The duration of the T = 298 K system was 9.4 μsec, the duration of the T = 328 K system was 6.9 μsec, and the duration of the $L_o$ control was 5.0 μsec.

## Local composition analysis

We calculated the locally averaged area density of DPPC on a 20 × 20 grid (roughly 5 Å between grid points), counting DPPC phosphates within 10 Å of each grid point for each simulation snapshot. This quantity we call $\rho(\mathbf{r})$, where $\mathbf{r}$ labels the grid point. To obtain a range for this observable that crosses zero at the average and has a range of order 1, we rescale this quantity by subtracting and dividing by the bulk average of $\rho(\mathbf{r})$: $\tilde{\rho}(\mathbf{r}) \equiv (\rho(\mathbf{r}) - \langle\rho\rangle)/\langle\rho\rangle$, where $\langle\rho\rangle$ is area density of DPPC averaged over the entire simulation cell. For this composition, $\langle\rho\rangle \approx 0.57\text{nm}^{-2}$. $\tilde{\rho}(\mathbf{r})$ ranges from −1 (no DPPC) to a (positive) maximum value that corresponds to the highest observed local density of DPPC, roughly 4 for both temperatures.

## Hidden Markov Model technical details

The HMM consists of two hidden states (putatively $L_o$ and $L_d$) and 28 emission signals (the 28 different local lipid compositions). For each lipid in each frame of simulation (sampled every 0.239 ns), the local composition is measured. The time-ordered local composition is the emission signal for that unknown state. Between each frame, the lipid may change state (e.g., $L_o$ to $L_d$) with a probability that does not depend on its history. There are four such so-called transition probabilities; each of the two states has a probability of changing or not changing state.

There are a total of 60 HMM parameters: 28 emission probabilities for each state and two transition probabilities for each state. The probabilities are constrained to sum to one, yielding 56 unique values to determine. These are determined by the Baum-Welch algorithm.[33,34] For some initial "guess" parameters, the algorithm computes the probability of observing the composition sequence given all possible sequences of states (summation over the astronomical number of paths is simplified by taking advantage of the Markovian character of the system via a forward-backward algorithm). The total expected number of emissions and transitions that occurred (summing over each possible path) are normalized and used as probabilities for the next iteration. Although an iteration is guaranteed to produce a more likely HMM, convergence to a global maximum is not guaranteed. Convergence of the parameters was checked by starting from ten initial guesses and selecting the best solution. In most cases a majority of the runs converged to nearly the same (most probable) model.

Once the HMM parameters are determined, the most likely state sequence is determined by the Viterbi algorithm,[35] which iterates through a sequence, saving (at each frame) the most likely state path to that frame from the start. Again, Markovian character is crucial to calculate the probability of a longer state sequence from the previous one.

A comparison of the HMM state assignment to the local density of DPPC and the thickness in each leaflet is shown for several configurations for $T < T_m$ (Fig. S2) and for $T > T_m$ (Fig. S3).

## Calculation of deuterium order parameters and quadrupolar spectra

Deuterium order parameters were calculated at each position along the aliphatic chains of DPPC according to

$$\langle |S_{cd}| \rangle = \frac{1}{2} \left\langle \left| 3\cos^2\theta - 1 \right| \right\rangle,$$

where $\theta$ is the angle between the carbon – hydrogen bond vector and the membrane normal, and the average is taken over snapshots separated by 2.4 nsec. The lipids are divided into two populations for the calculation based on the Hidden Markov Model analysis. The left and right panels of Figure S4 present the order parameters for the $T < T_m$ and $T > T_m$ system, respectively.

### Calculation of $^2$H NMR spectra

The simulated spectra were calculated according to the formula

$$\Delta\nu_q(n) = \frac{3}{4}\frac{e^2qQ}{h}S(n),$$

where $\Delta\nu_q(n)$ are the quadrupolar splittings for each methylene- and methyl group of *sn*-1 and *sn*-2 hydrocarbon chains, $e^2qQ/h$=167 kHz, and $S(n)$ are the order parameters from the simulation. A random distribution of orientations of bilayer normals to the magnetic field was assumed.

### Extraction of $S_{CD}$ values from experimentally measured $^2$H spectra

The order parameters of hydrocarbon chains of DPPC in the spectrum of coexisting $L_d$ and $L_o$ phases were extracted by choosing a pure $L_d$ phase spectrum recorded at higher temperature that perfectly matched the $L_d$ component in the $L_d$/$L_o$ spectrum. After intensity adjustment, this $L_d$ spectrum was subtracted to yield the spectrum of the pure $L_o$ component. Order parameters were extracted from the $L_d$ and $L_o$ spectra by integration as described earlier.[36] A few resolved quadrupolar splittings were assigned directly. The quality of order parameter extraction was verified by comparing measured and simulated spectra of $L_d$/$L_o$ phase coexistence.

### Calculation of lipid-lipid pair contact frequencies

Lipid-lipid and lipid-cholesterol boundaries are mapped by identifying pairs that share a boundary in a Voronoi tessellation of a configuration. The sample of configurations then provides information on the statistics of pairwise contacts. The extent to which the observed interaction statistics deviate from a random mixture is found by comparison to randomized configurations, under the constraint that the composition remains fixed. Two null hypotheses were considered: Randomization over the entire system, and randomization within each phase.

## RESULTS

### Lipids mix laterally on 10 µsec timescales

An initial configuration for a $L_o$ nanodomain was prepared by embedding a 5 nm diameter $L_o$ region in a 10 nm × 10 nm $L_d$ bilayer (Fig. S1). The compositions of the two phases were set to the experimentally determined compositions for a ternary mixture of DOPC/DPPC/ cholesterol just below the miscibility transition.[13] (Details on the system set up and simulation protocol are found in Supplementary Materials (SM).) Fig. 1 illustrates the extent to which the lipids initially in the $L_o$ domain have mixed by the end of the simulation. This may be quantified by asking the question: what is the probability of finding an original $L_o$ lipid at a distance *r* from another original $L_o$ lipid? Comparing cumulative distribution functions for these lipids (CDF) averaged over the first 100 nsec of the simulation and the last 100 nsec, it is clear that the initial domain of $L_o$ lipids has dispersed (Fig. S2). Furthermore, comparison to the CDF of an equal number of randomly selected lipids shows

that by the end of the simulation the initially $L_o$ lipids have mixed (dotted line in Fig. S2), indicating that the simulation time-scale is sufficient to sample compositional degrees of freedom.

### Local composition reveals a stable domain for $T < T_m$

Experimentally, it is known that the $L_o$ and $L_d$ regions differ in composition, with the $L_o$ region comparatively enriched in DPPC and cholesterol. Whether a particular lipid belongs to the $L_o$ or the $L_d$ region should therefore be encoded in the composition of its local neighborhood. A neighborhood enriched in DPPC and cholesterol is more likely to be in the $L_o$ phase than $L_d$, but how much more likely?

This was answered by developing a hidden Markov model (HMM) for the local membrane phase. The local composition in the vicinity of each lipid (determined by the six nearest lipids in the same leaflet, including itself) is recorded in a time series (one for each lipid). This "observable" data is used to define two "hidden" states (putatively $L_o$ or $L_d$.). The parameters of the model are the probabilities of each hidden state to have a certain lipid composition, and the probabilities for a hidden state to change to the other in one time step. The values of the unknown probabilities were determined by the requirement that they maximize the likelihood of the observed sequence of 39,272 compositions for each of the 348 lipids using standard methods for solving HMMs. The HMM can also be used to define the hidden state at any point in the bilayer, given a local lipid composition. (See Methods for complete details.)

The result of the HMM analysis is a map of each leaflet of the bilayer onto $L_o$ and $L_d$ phases; a representative configuration is shown in the top panels of Fig. 2. The bilayer phase determined by the HMM analysis is consistent with a direct analysis of the local composition and the bilayer thickness (middle and bottom panels of Fig. 2, and **S3**), both of which are markers of the $L_o$ phase. It is clear that despite extensive mixing of the lipids, a local region with features consistent with the $L_o$ phase persists throughout the simulation.

The simulation admits direct observation of the dynamics of nanoscale $L_o/L_d$ coexistence, included as a web enhanced object, with the rendering explained in the caption to Figure 4. ("lowT_small.mpeg") The persistence of the $L_o$ region is apparent, as is the exchange of lipids between the regions. Transient hexagonal structures are observed within the $L_o$ region, discussed in more detail below.

In contrast, a simulation of the homogeneous phase above the miscibility transition temperature reveals compositional fluctuations that at times appear $L_o$-like, yet occur on a much faster timescale (Fig. S4 and movie available as a web enhanced object "highT_small.mpeg"). Despite a similar structure in the lateral composition, the $T > T_m$ data have distinctly different structure in the hydrocarbon chains, described next.

### Deuterium quadrupolar splittings confirm $L_o/L_d$ coexistence

Based on the assignment of each lipid into either the $L_o$ or $L_d$ phase, we computed the C-D order parameters of DPPC hydrocarbon chains ($S_{CD}$) at each position for both temperatures (Fig. S5). $S_{CD}$ reports the average alignment of the carbon-hydrogen covalent bonds relative

to the bilayer normal, and is proportional to the quadropolar splitting of resonances observed in a $^2$H NMR experiment on samples containing DPPC with perdeuterated hydrocarbon chains. The quadrupolar splittings therefore distinguish the $L_o$ and $L_d$ phases by virtue of the more ordered chains in the $L_o$ phase—indeed, this feature is the origin of the word "ordered" in "liquid ordered phase."

In order to facilitate comparison to the experimental data, $^2$H NMR spectra were computed from the simulated order parameters as described in Methods. The simulated and measured spectra are shown in Fig. 3. The central resonances corresponding to the terminal methyls (red arrows in the bottom panel of Fig. 3) show a characteristic triple peak structure below $T_m$, but yield a single splitting above $T_m$. In the $L_o$ phase ($T < T_m$), the lipids are oriented parallel to the bilayer normal with more ordered chains. Consequently, the *sn*-1 chain protrudes more deeply into the bi-layer center than the *sn*-2 chain, yielding distinct splittings and producing the two outer pairs of peaks below $T_m$. In the $L_d$ phase the chains are disordered and the terminal methyls produce a single splitting corresponding to the innermost pair of peaks. The resonances arising from the rest of the carbons below $T_m$ overlap and are difficult to distinguish on a carbon-by-carbon basis, but they yield two distinct populations, indicated by the two broad shoulders in the wings of the spectra. By comparison, the high T data in Fig. 3 are consistent with a single population of lipids without any components that are distinguishable on the NMR timescale of about 10 μsec. Table 1 compares the average order parameters from simulation and experiment. The chains of the $L_o$ phase are slightly less ordered on average than reported by the experiment, most likely due to the high fraction of lipids at the $L_o/L_d$ boundary in the $T < T_m$ simulation. Indeed, the average order parameters observed in a control simulation of the $L_o$ phase are in excellent agreement with the experimentally measured values. The compositions of the two phases also agree with those measured experimentally [13] (Table 2), except for the balance of DOPC to DPPC in the $L_d$ phase.

### Substructure composed of aligned alkyl chains with locally hexagonal order is observed in the $L_o$ phase

Visualization of the centers of mass of the hydrocarbon chains and cholesterol reveals a local, approximately hexagonal substructure within the $L_o$ phase, comprised of regions of densely packed DPPC chains, shown in Fig. 4A and in the web enhanced object discussed above. Similar substructure is observed in the $L_o$ control simulation (Figs. 4B, 4C). A movie corresponding to Fig. 4B is available as a web enhanced object ("LoControl_small.mpeg"). These regions are composed of lipids with aligned saturated chains oriented parallel to the bilayer normal, as shown in the molecular graphic (Fig. 4C). They have *sn*-1- and *sn*-2 hydrocarbon chains with distinctly different quadropolar splittings of terminal methyl groups as measured for the $L_o$ phase. The substructure is nonetheless fluid — the order does not extend over long range, it is dynamic, and analysis of the lifetimes of saturated chain contacts shows that contacts deepest in the hexagonal regions of the $L_o$ domain have a lifetime of approximately 400 nsec (Fig. 5). Despite the compositional fluctuations that mimic the $L_o$ phase, aligned chains, persistent contacts, and locally hexagonal order are not observed above $T_m$.

Because the simulation timescale admits thorough sampling of the compositional degrees of freedom, the statistics of lipid interactions may be addressed directly; here the frequencies of lipid-lipid contacts are analyzed, as measured by boundary lengths in a Voronoi tesselation. These boundary lengths are compared to the expected lengths for random distributions (ideal mixing) over the entire system and within each phase (Table 3, details in Methods). In every case, nearest neighbor cholesterol-cholesterol interactions are strongly disfavored, consistent with previous simulation results for binary mixtures.[20] Within the $L_o$ phase, the local hexagonal structure is reflected in the frequency of DPPC-DPPC contacts, which are enhanced relative to ideal mixing. Cholesterol boundaries were distingiushed between the smooth and rough faces (S and R in Table 3). Within the $L_o$ region, cholesterol-DPPC contacts favor the smooth face, while cholesterol-DOPC contacts favor the rough face. Taken together, these data indicate that cholesterol mediates the boundary between the locally hexagonal regions in the $L_o$ phase and the interstitial, more disordered regions, and that it does so by virtue of its two (α and β) faces.

## DISCUSSION AND CONCLUSIONS

The simulation data reveal substructure within the $L_o$ phase—local regions of hexagonally ordered saturated chains are separated by interstitial regions enriched in cholesterol. This picture of the $L_o$ phase provides an explanation for a number of experimental results, which have until now lacked a consistent description in terms of a molecular model:

### $^2$H NMR quadropolar splittings

Distinct splittings of the *sn*-1 and *sn*-2 DPPC terminal methyls are produced by very ordered hydrocarbon chains aligned parallel to the bilayer normal. This is a distinguishing characteristic for detection of $L_o$ phases. Although the hydrocarbon chains have high order, characteristic of chains with few if any gauche defects, the spectra still indicate rapid reorientation about the bilayer normal of lipids as individual molecules or small clusters. Furthermore, for resolved resonances only one set of quadrupolar splittings per methyl- or methylene group is detected, indicating that the chains explore their entire configurational space on the NMR timescale (correlation times less than 10 μsec). This imposes strong limits on aggregate size.[13] In summary, the experimental spectra are in excellent agreement with organization of DPPC in small, highly mobile clusters with hydrocarbon chains packed in a hexagonal lattice and rapid exchange of DPPC molecules.

### $^1$H magic-angle spinning NMR

The chain methylene resonances of DPPC in the $L_d$ phase have a typical linewidth of 50–100 Hz. They broaden by a factor of ten in the $L_o$ phase compared to $L_d$. This is the result of greatly reduced trans-gauche isomerization of chains, consistent with the arrangement of DPPC in mostly trans hexagonally ordered regions.[37]

### NMR diffusion measurements

Mean squared displacements are reduced by roughly a factor of 3 in $L_o$ compared to $L_d$.[38] This is consistent with the slower (but still liquid-like) diffusion observed in $L_o$, clearly evident in the movie of the $L_o$ phase accompanying Fig. 4.

### Small angle X-ray scattering

Bilayer thickness is increased and area per lipid decreased in $L_o$,[39] due to regions of packed DPPC chains.

### Small angle neutron scattering

Nanoscale domains with hexagonal order have recently been reported in binary mixtures of DPPC with cholesterol.[40]

The composition and cholesterol dependence of the $L_o$ phase evoke nanoscale size raft regions in the cell membrane, and yet membrane components that partition to raft regions in cell membranes typically do not partition to the $L_o$ phase in bilayers.[6,41] Since many putative raft components have a preference for solvation by cholesterol, within the $L_o$ phase they should partition to the cholesterol rich regions found at the boundaries of the densely packed hexagonal DPPC clusters. In the macroscopic $L_o$ phase observed below $T_m$ for mixtures of DPPC, DOPC, and cholesterol, there is comparatively little cholesterol rich area available to solvate such components. In the resting cell membrane, however, raft regions are known to be quite small,[9,10] consistent instead with nanoscale clusters of ordered chains, solvated by a cholesterol rich boundary region. These nanoscale clusters may be driven by $T > T_m$ composition fluctuations, stabilized by immobilized "defects",[42] or they may be a result of reduced line tension from replacing DOPC by POPC.[14] Since many small nanoscale clusters have an increased total boundary length relative to a macroscopic phase, components favoring cholesterol would find more such regions accessible. Furthermore, the size and balance of substructure within such regions (and therefore the area available to solvate raft components) in the cell membrane may well be shifted by several mechanisms, including coupling to the cytoskeleton,[42–44] proximity to the miscibility transition,[11,13,45] or active maintenance by the cell.[46,47] Indeed, crosslinking of components that partition into the densely packed substructure provides a natural mechanism to trigger small clusters to coalesce into a macroscopic domain.[41] Thus, understanding precisely how the $L_o$ substructure is altered by such mechanisms presents itself as a promising line of inquiry to resolve the connection between lipid bilayer and cell membrane lateral structure.

But why then is cholesterol a necessary component for liquid-liquid coexistence? Beginning with early work on *binary mixtures* of cholesterol and saturated phospholipids,[48–50] it has been hypothesized that the structure and thermodynamics of the $L_o$ phase are driven by direct interactions between cholesterol and saturated lipids. This idea has been elaborated by McConnell and Radhakrishnan in terms of "condensed complexes."[51] The condensed complex model departs from regular solution theory by including a fourth species to model a stoichiometric condensed complex of cholesterol and (in this case) DPPC. An alternate view that proposes a longer range, lattice-like substructure in the $L_o$ phase of binary mixtures containing cholesterol has been proposed by Chong and coworkers, with the lattice composed of condensed complexes of lipid and cholesterol.[52]

In contrast, the present results indicate that cholesterol disrupts what would otherwise be gel-fluid coexistence, not just by direct interactions with the lipids, but indirectly, because cholesterol prefers an organization that is incommensurate with the local order preferred by

DPPC in the $L_o$ phase. Consistent with this idea, Martinez-Seara, et al.[20] recently showed that when in binary mixtures with DSPC, cholesterol prefers to interact with other cholesterols in next-nearest neighbor solvation shells at three-fold symmetric orientations, but the acyl chains of DSPC lie at roughly five-fold symmetric positions around cholesterol. Consequently, the rotational symmetry of cholesterol in $L_o$ regions appears to be only partially compatible with hexagonally ordered DPPC chains. One may then view the condensed complex model as a way to incorporate non-mean field density fluctuations into regular solution theory. The present data indicate that these non-mean field fluctuations are not stoichiometric complexes of cholesterol with DPPC, but, rather, DPPC with itself. Indeed, more than 20 years ago Sankaram and Thompson suggested, on the basis of $^2H$ NMR spectra and electron spin resonance measurments of binary mixtures, that the data could be explained not by stoichiometric complexes but by time averaged cholesterol positions.[53,54] This hypothesis could be tested by calculations similar to those presented here, replacing cholesterol by other sterols, such as lanosterol. Published 2H NMR[55] and quasi-elastic neutron scattering[56] studies report sterol-dependent differences in the ordering and dynamics of the lipid chains.

In summary, the $L_o$ phase of a mixture of cholesterol and two lipids is shown to be itself inhomogeneous. Lateral segregation within the $L_o$ phase is observed, with regions of hexagonally packed saturated chains separated by insterstital regions enriched in cholesterol and unsaturated chains. The observed substructure explains existing experimental data, and provides a focus for future efforts aimed at understanding the molecular scale structure of cell membranes.

## Supplementary Material

Refer to Web version on PubMed Central for supplementary material.

## Acknowledgments

## References

1. Shimshick EJ, McConnell HM. Biochemistry. 1973; 12:2351. [PubMed: 4351059]

2. Feigenson GW. Annual Review of Biophysics and Biomolecular Structure. 2007; 36:63.

3. Veatch SL, Keller SL. Biochimica et Biophysica Acta (BBA) - Molecular Cell Research. 2005; 1746:172.

4. Bartels T, Lankalapalli RS, Bittman R, Beyer K, Brown MF. Journal of the American Chemical Society. 2008; 130:14521. [PubMed: 18839945]

5. Hjort Ipsen J, Karlström G, Mourtisen OG, Wennerström H, Zuckermann MJ. Biochimica et Biophysica Acta (BBA) - Biomembranes. 1987; 905:162.

6. Lingwood D, Simons K. Science. 2010; 327:46. [PubMed: 20044567]

7. Pike LJ. Journal of Lipid Research. 2006; 47:1597. [PubMed: 16645198]

8. Simons K, Ikonen E. Nature. 1997; 387:569. [PubMed: 9177342]

9. Eggeling C, Ringemann C, Medda R, Schwarzmann G, Sandhoff K, Polyakova S, Belov VN, Hein B, von Middendorff C, Schonle A, Hell SW. Nature. 2009; 457:1159. [PubMed: 19098897]

10. Sezgin E, Levental I, Grzybek M, Schwarzmann G, Mueller V, Honigmann A, Belov VN, Eggeling C, Coskun Ü, Simons K, Schwille P. Biochimica et Biophysica Acta (BBA) - Biomembranes. 2012; 1818:1777.

11. Veatch SL, Cicuta P, Sengupta P, Honerkamp-Smith A, Holowka D, Baird B. ACS Chemical Biology. 2008; 3:287. [PubMed: 18484709]

12. Honerkamp-Smith AR, Cicuta P, Collins MD, Veatch SL, den Nijs M, Schick M, Keller SL. Biophysical journal. 2008; 95:236. [PubMed: 18424504]

13. Veatch SL, Soubias O, Keller SL, Gawrisch K. Proc Nat Acad Sci. 2007; 104:17650. [PubMed: 17962417]

14. Heberle FA, Petruzielo RS, Pan J, Drazba P, Kučerka N, Standaert RF, Feigenson GW, Katsaras J. Journal of the American Chemical Society. 2013; 135:6853. [PubMed: 23391155]

15. Zhao J, Wu J, Heberle FA, Mills TT, Klawitter P, Huang G, Costanza G, Feigenson GW. Biochimica et Biophysica Acta (BBA) - Biomembranes. 2007; 1768:2764.

16. Heberle FA, Wu J, Goh SL, Petruzielo RS, Feigenson GW. Biophysical journal. 2010; 99:3309. [PubMed: 21081079]

17. Konyakhina TM, Goh SL, Amazon J, Heberle FA, Wu J, Feigenson GW. Biophysical journal. 2011; 101:L8. [PubMed: 21767476]

18. Róg T, Pasenkiewicz-Gierula M, Vattulainen I, Karttunen M. Biochimica et Biophysica Acta (BBA) - Biomembranes. 2009; 1788:97.

19. Khelashvili G, Pabst G, Harries D. The Journal of Physical Chemistry B. 2010; 114:7524. [PubMed: 20518573]

20. Martinez-Seara H, Róg T, Karttunen M, Vattulainen I, Reigada R. PLoS ONE. 2010; 5:e11162. [PubMed: 20567600]

21. Róg T, Pasenkiewicz-Gierula M. Biophysical journal. 2001; 81:2190. [PubMed: 11566790]

22. Waheed Q, Tjörnhammar R, Edholm O. Biophysical journal. 2012; 103:2125. [PubMed: 23200046]

23. Perlmutter JD, Sachs JN. Journal of the American Chemical Society. 2009; 131:16362. [PubMed: 19860442]

24. Pandit SA, Vasudevan S, Chiu SW, Jay Mashl R, Jakobsson E, Scott HL. Biophysical journal. 2004; 87:1092. [PubMed: 15298913]

25. Niemelä PS, Ollila S, Hyvönen MT, Karttunen M, Vattulainen I. PLoS Comput Biol. 2007; 3:e34. [PubMed: 17319738]

26. Alameida, PFF.; Vaz, WLC. Handbook of Biological Physics. Lipowsky, R.; Sackman, E., editors. Vol. 1. Elsevier Science B.V; Amsterdam: 1995. p. 305

27. de Joannis J, Coppock PS, Yin F, Mori M, Zamorano A, Kindt JT. Journal of the American Chemical Society. 2011; 133:3625. [PubMed: 21341653]

28. Shaw DE, Maragakis P, Lindorff-Larsen K, Piana S, Dror RO, Eastwood MP, Bank JA, Jumper JM, Salmon JK, Shan Y, Wriggers W. Science. 2010; 330:341. [PubMed: 20947758]

29. Jo S, Kim T, Iyer VG, Im W. Journal of Computational Chemistry. 2008; 29:1859. [PubMed: 18351591]

30. Shaw, DE.; Dror, RO.; Salmon, JK.; Grossman, JP.; Mackenzie, KM.; Bank, JA.; Young, C.; Deneroff, MM.; Batson, B.; Bowers, KJ.; Chow, E.; Eastwood, MP.; Ierardi, DJ.; Klepeis, JL.; Kuskin, JS.; Larson, RH.; Lindorff-Larsen, K.; Maragakis, P.; Moraes, MA.; Piana, S.; Shan, Y.; Towles, B. Proceedings of the Conference on High Performance Computing Networking, Storage and Analysis. ACM; Portland, Oregon: 2009. p. 1

31. Martyna GJ, Tobias DJ, Klein ML. The Journal of Chemical Physics. 1994; 101:4177.

32. Shan Y, Klepeis JL, Eastwood MP, Dror RO, Shaw DE. The Journal of Chemical Physics. 2005; 122:054101.

33. Baum LE, Petrie T, Soules G, Weiss N. Ann Math Stat. 1970; 41:164.

34. Welch LR. IEEE Info Theo Soc News. 2003; 53:4.

35. Viterbi AJ. IEEE Trans Info Theo. 1967; 13:260.

36. Lafleur M, Cullis PR, Bloom M. Eur Biophys J. 1990; 19:55. [PubMed: 2073890]

37. Polozov IV, Bezrukov L, Gawrisch K, Zimmerberg J. Nat Chem Biol. 2008; 4:248. [PubMed: 18311130]

38. Orädd G, Westerman PW, Lindblom G. Biophysical journal. 2005; 89:315. [PubMed: 15863478]

39. Mills TT, Tristram-Nagle S, Heberle FA, Morales NF, Zhao J, Wu J, Toombes GES, Nagle JF, Feigenson GW. Biophysical journal. 2008; 95:682. [PubMed: 18390623]

40. Armstrong CL, Marquardt D, Dies H, Kučerka N, Yamani Z, Harroun TA, Katsaras J, Shi AC, Rheinstädter MC. PLoS ONE. 2013; 8:e66162. [PubMed: 23823623]

41. Hammond AT, Heberle FA, Baumgart T, Holowka D, Baird B, Feigenson GW. Proceedings of the National Academy of Sciences of the United States of America. 2005; 102:6320. [PubMed: 15851688]

42. Zhao J, Wu J, Veatch SL. Biophysical journal. 2013; 104:825. [PubMed: 23442961]

43. Kusumi A, Fujiwara TK, Morone N, Yoshida KJ, Chadda R, Xie M, Kasai RS, Suzuki KGN. Seminars in Cell & Developmental Biology. 2012; 23:126. [PubMed: 22309841]

44. Kusumi A, Sako Y. Current Opinion in Cell Biology. 1996; 8:566. [PubMed: 8791449]

45. Fan J, Sammalkorpi M, Haataja M. Physical Review Letters. 2010; 104:118101. [PubMed: 20366502]

46. Fan J, Sammalkorpi M, Haataja M. Physical Review Letters. 2008; 100:178102. [PubMed: 18518341]

47. Gowrishankar K, Ghosh S, Saha S, CR, Mayor S, Rao M. Cell. 2012; 149:1353. [PubMed: 22682254]

48. Gershfeld NL. Biophysical journal. 1978; 22:469. [PubMed: 667296]

49. Hinz HJ, Sturtevant JM. Journal of Biological Chemistry. 1972; 247:3697. [PubMed: 5030639]

50. Presti FT, Pace RJ, Chan SI. Biochemistry. 1982; 21:3831. [PubMed: 7138808]

51. Radhakrishnan A, McConnell H. Proceedings of the National Academy of Sciences of the United States of America. 2005; 102:12662. [PubMed: 16120676]

52. Sugár IP, Chong PLG. Journal of the American Chemical Society. 2011; 134:1164. [PubMed: 22196210]

53. Sankaram MB, Thompson TE. Biochemistry. 1990; 29:10676. [PubMed: 2271675]

54. Sankaram MB, Thompson TE. Proceedings of the National Academy of Sciences. 1991; 88:8686.

55. Martinez GV, Dykstra EM, Lope-Piedrafita S, Brown MF. Langmuir. 2004; 20:1043. [PubMed: 15803674]

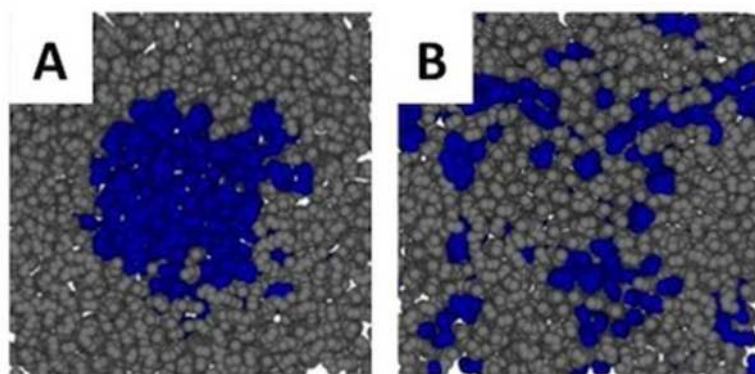56. Endress E, Heller H, Casalta H, Brown MF, Bayerl TM. Biochemistry. 2002; 41:13078. [PubMed: 12390036]

**Figure 1.**
The lipids initially in the $L_o$ domain (blue, Panel A) have mixed by the end of the simulation (Panel B). The cumulative distribution function (Fig. S2) of the lipids initially in the $L_o$ region confirms that by the end of the 10 μsec simulation these lipids are indistinguishable from the same number of randomly chosen lipids.
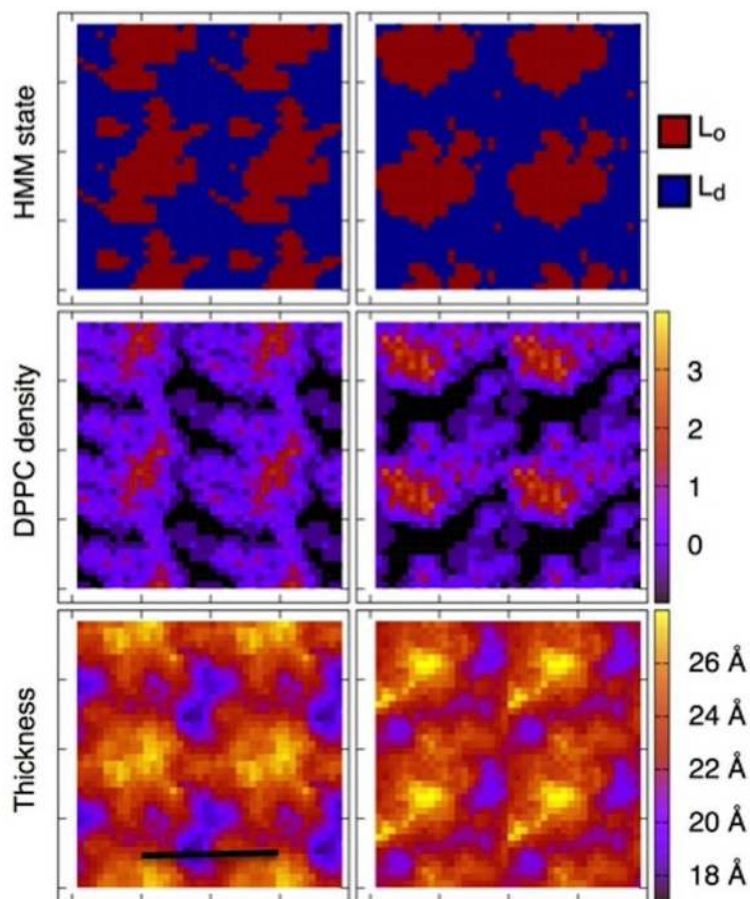
**Figure 2.**
Hidden Markov model analysis reveals a robust domain despite extensive lipid mixing. The region identified as $L_o$ by the HMM analysis coincides with a region of enhanced DPPC density (black is no DPPC, and the bulk average DPPC density corresponds to zero on the unitless color scale, defined in Methods), and increased per leaflet membrane thickness. Three periodic images are shown in addition to the simulation cell, the scale bar is 10 nm. Top leaflet is on the left, and bottom is on the right.
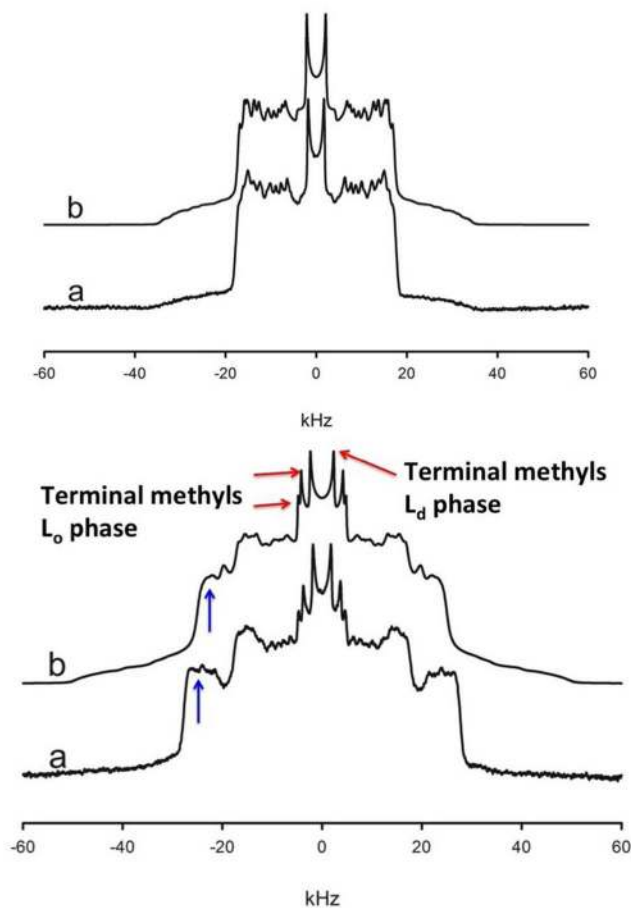
**Figure 3.**
Comparison of experimental (a) and simulated (b) $^2H$ NMR spectra of DPPC with perdeuterated hydrocarbon chains for $T < T_m$ (bottom panel) and $T > T_m$ (top panel). The low T spectra show the features characteristic of $L_o/L_d$ coexistence. The terminal methyls produce one pair of peaks for the $L_d$ phase (central pair of peaks) and two pairs (one each for the *sn*-1 and *sn*-2 chains) for the $L_o$ phase. The rest of the carbons produce two broad bands of peaks arising from overlapping and broadened resonances, with the inner band arising from the $L_d$ phase. The broad shoulder arising from the $L_o$ upper chain methylenes (blue arrows) produce a slightly narrower splitting in the simulated spectrum, indicating slightly less order in the simulation than in the experiment. The best match between the high T simulation data (328 K) and experimental spectrum is found for experimental data acquired at 313 K, indicating a shift in the temperature dependence of the model for $T > T_m$.
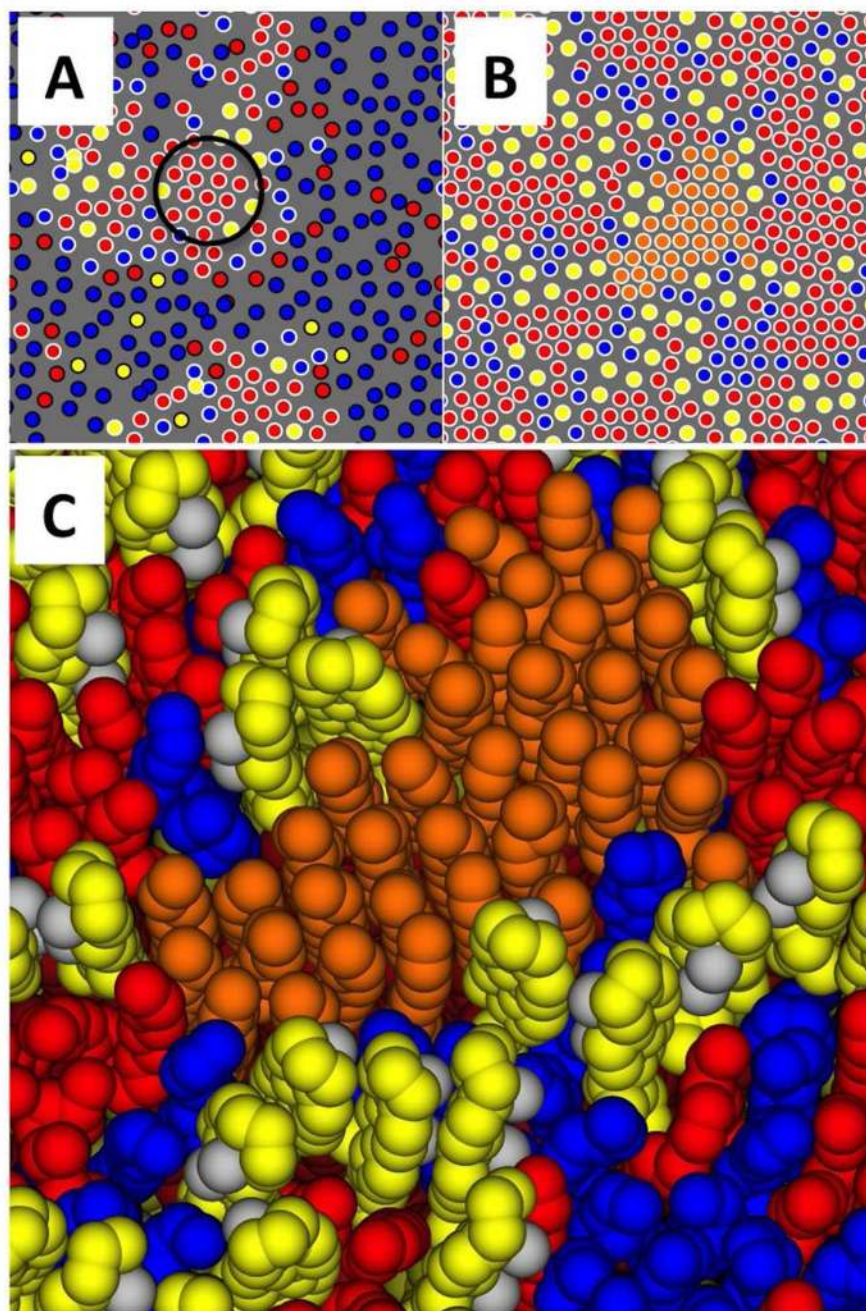
**Figure 4.**
Center of mass locations of lipid chains and cholesterol for one leaflet of the $L_o/L_d$ simulation at 298 K (A) and the $L_o$ control (B). DPPC chains red, DOPC chains blue, and cholesterol yellow, no periodic images are shown. In panel A, lipids identified as $L_o$ by the HMM analysis are indicated by a white border, and $L_d$ lipids are indicated by a black border. An area of locally hexagonal order is observed within the $L_o$ region, indicated by the black circle. Within such regions, DPPC chains are well-ordered and pack tightly. The control simulation (panel B) reveals multiple locally hexagonal regions, bounded by areas enriched

in cholesterol and DOPC. The molecular detail in one such region, highlighted in orange, is shown in panel C. Methyl groups on the β face of the cholesterols are colored gray, headgroups are not rendered in order to reveal the chain structure.
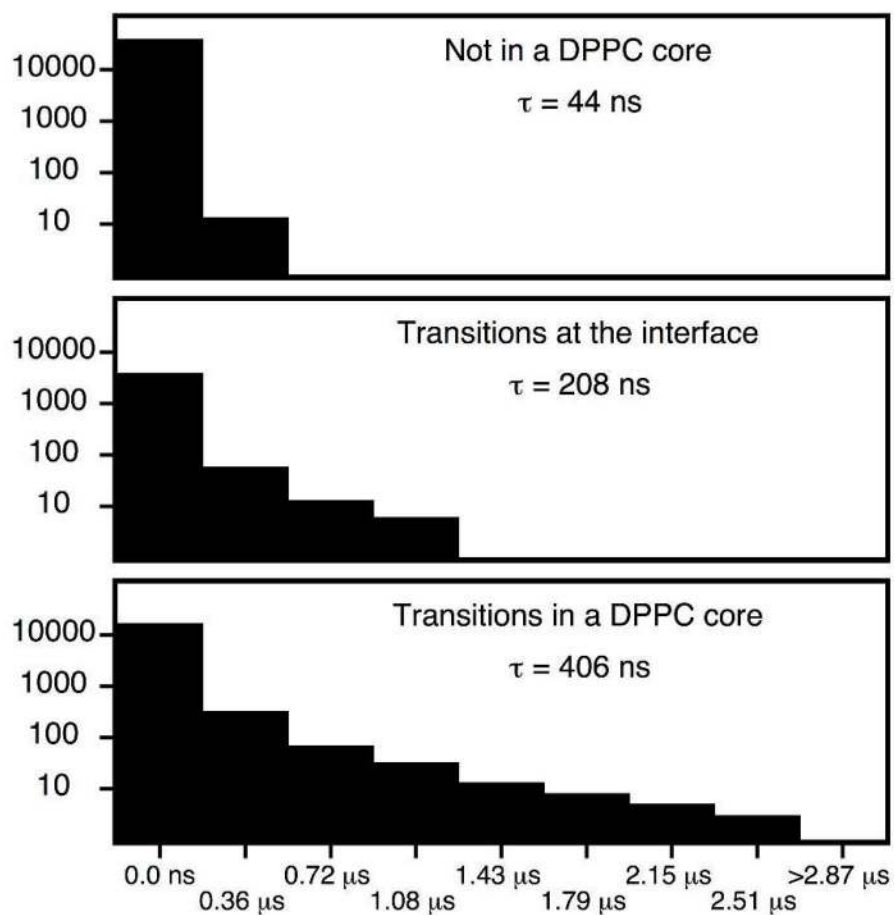
**Figure 5.**
Histograms of aligned chain contact lifetimes. Aligned DPPC chain contacts display a distribution of lifetimes which depends on where the chain contacts are observed. Chain contacts in the locally hexagonal core have the longest lifetime

**Table 1**

Comparison of experimentally measured and simulated $^2$H NMR order parameters at 298 K. Order parameters are averaged over all carbons in both sn-1 and sn-2 chains. The experimental order parameters were obtained from the spectra as described in Methods. Standard errors are indicated in the parentheses.

|       | Expt. | $L_o/L_d$Sim. | Control Sim. |
|-------|-------|---------------|--------------|
| $L_o$ | 0.36  | 0.321(0.003)  | 0.373(0.001) |
| $L_d$ | 0.21  | 0.208(0.001)  | 0.223(0.001) |

**Table 2**

Fractional compositions of the two phases determined by experiment[13] and simulation. Standard errors are reported in parentheses.

|  | CHL | DPPC | DOPC |
|---|---|---|---|
| $L_o$ (expt.) | 0.31 | 0.55 | 0.15 |
| $L_o$ (sim.) | 0.27(0.2) | 0.51(0.4) | 0.22(0.3) |
| $L_d$ (expt.) | 0.11 | 0.29 | 0.60 |
| $L_d$ (sim.) | 0.08(0.2) | 0.16(0.4) | 0.75(0.5) |

**Table 3**

Percentage change in the length of lipid-lipid boundaries, relative to a randomly mixed system. Boundaries with the (S)mooth and (R)ough faces of cholesterol are considered separately. The column labeled $L_o/L_d$ corresponds to the $T < T_m$ phase separated system, $L_o$ is the $L_o$ control, and $L_d$ is the $L_d$ control. The values in parentheses are the standard errors of 10 non overlapping blocks of data.

|  | $L_o/L_d$ | $L_o$ | $L_d$ |
|---|---|---|---|
| **CHL(S)-DPPC** | +31.8(1.2) | +19.0(1.2) | −26.7(1.7) |
| **CHL(S)-DOPC** | −14.8(1.7) | +6.9(1.7) | +2.0(1.0) |
| **CHL(R)-DPPC** | +25.2(1.2) | +12.7(1.6) | −28.9(1.2) |
| **CHL(R)-DOPC** | +0.7(1.3) | +37.1(1.7) | +11.2(1.2) |
| **CHL(S)-CHL(S)** | +12.6(3.2) | +3.8(1.7) | −54.2(3.2) |
| **CHL(S)-CHL(R)** | −12.0(2.7) | −18.8(1.7) | −66.0(2.0) |
| **CHL(R)-CHL(R)** | −42.6(1.7) | −47.1(1.4) | −76.2(1.8) |
| **DPPC-DPPC** | +25.6(2.8) | +12.8(1.8) | −20.2(1.5) |
| **DPPC-DOPC** | −25.1(1.7) | −20.3(1.9) | +0.15(0.7) |
| **DOPC-DOPC** | +19.9(1.2) | −22.3(1.9) | +4.2(0.3) |